



HAL
open science

Silicon isotope measurement in zircon by laser ablation multiple collector inductively coupled plasma mass spectrometry

Martin Guitreau, Abdelmouhcine Gannoun, Zhengbin Deng, Johanna Marin-Carbonne, Marc Chaussidon, Frédéric Moynier

► To cite this version:

Martin Guitreau, Abdelmouhcine Gannoun, Zhengbin Deng, Johanna Marin-Carbonne, Marc Chaussidon, et al.. Silicon isotope measurement in zircon by laser ablation multiple collector inductively coupled plasma mass spectrometry. *Journal of Analytical Atomic Spectrometry*, 2020, 35 (8), pp.1597-1606. 10.1039/D0JA00214C . hal-02944428

HAL Id: hal-02944428

<https://uca.hal.science/hal-02944428>

Submitted on 23 Sep 2020

HAL is a multi-disciplinary open access archive for the deposit and dissemination of scientific research documents, whether they are published or not. The documents may come from teaching and research institutions in France or abroad, or from public or private research centers.

L'archive ouverte pluridisciplinaire **HAL**, est destinée au dépôt et à la diffusion de documents scientifiques de niveau recherche, publiés ou non, émanant des établissements d'enseignement et de recherche français ou étrangers, des laboratoires publics ou privés.

1 Silicon isotope measurement in zircon by laser ablation
2 multiple collector inductively coupled plasma mass
3 spectrometry

4

5 **Martin Guitreau^{1*}, Abdelmouhcine Gannoun¹, Zhengbin Deng^{2**}, Johanna Marin-
6 Carbonne³, Marc Chaussidon², Frédéric Moynier²**

7

8 ¹ *Université Clermont Auvergne, CNRS, IRD, OPGC, Laboratoire Magmas et Volcans, UMR 6524, F-
9 63000, Clermont-Ferrand, France.*

10 ² *Université de Paris, Institut de Physique du globe de Paris, CNRS UMR 7154, 75005 Paris, France*

11 ³ *Institut des Sciences de la Terre, Université Lausanne, Géopolis Mouline, 1015 Lausanne,
12 Switzerland*

13

14 ** Correspondence: martin.guitreau@uca.fr*

15 *** Present address: Centre for Star and Planet Formation, Globe Institute, University of Copenhagen,
16 Copenhagen, Denmark*

17

18 **Keywords:** stable Si isotopes, Zircon, LA-MC-ICP-MS

19

20

21

22 **ABSTRACT**

23 **This study reports the first Si isotope data measured in zircon using nanosecond
24 laser ablation multiple collector inductively coupled plasma mass spectrometry.**

25 **Long-term (>2 years) external reproducibility obtained on the 91500 zircon
26 standard is 0.13‰ and 0.21‰ (2SD) for $\delta^{29}\text{Si}$ and $\delta^{30}\text{Si}$ (per mil deviation from the**

27 quartz reference NBS 28), respectively, and typical precision on a single run is on
28 the order of 0.10‰ and 0.12‰ (2SE) for $\delta^{29}\text{Si}$ and $\delta^{30}\text{Si}$, respectively. Our results
29 show good consistency between laser ablation multiple collector inductively
30 coupled plasma mass spectrometry (LA-MC-ICP-MS) and solution multiple
31 collector inductively coupled plasma mass spectrometry (S-MC-ICP-MS) /
32 secondary ionization mass spectrometry (SIMS) data demonstrating that the Si
33 isotopic composition of zircon can be accurately measured by LA-MC-ICP-MS.
34 Obtained $\delta^{30}\text{Si}$ values on natural zircon standards range from $-0.32 \pm 0.23\text{‰}$ (2SD)
35 for 91500 to $-0.47 \pm 0.17\text{‰}$ for MudTank, whereas the MUN (synthetic) zircon
36 standards have lower $\delta^{30}\text{Si}$ values around -2.0‰ (e.g. $-2.08 \pm 0.17\text{‰}$ for MUN-1-
37 2b). Silicon isotope measurements by LA-MC-ICP-MS open new possibilities for
38 studying zircon formation in various geological contexts.

39

40 1. Introduction

41 Silicon is the third most abundant element on Earth (e.g., [McDonough, 2003](#)) and it
42 commonly bonds with oxygen to form SiO_4 tetrahedrons that represent the building
43 blocks of all silicates. Silicon is therefore deeply involved in a lot of processes within
44 and at the surface of the Earth. Silicon has three stable isotopes; ^{28}Si (92.23%), ^{29}Si
45 (4.68%), and ^{30}Si (3.09%), and the measurement of their relative abundances has long
46 been developed for various applications in planetary and Earth sciences, as well as in
47 biological and environmental studies (e.g., [Poitrasson, 2017](#); [Ding et al., 2018](#); [Sutton
48 et al., 2018](#)). Most studies have focused on bulk sample measurement (e.g., [Clayton et
49 al., 1978](#); [Ziegler et al., 2005](#); [André et al., 2006](#); [Van den Boorn et al., 2010](#); [Savage
50 et al., 2011](#); [Opfergelt et al., 2012](#); [Zambardi et al., 2013](#); [Deng et al., 2019](#)) but
51 analytical development and scientific needs have conducted to the analysis of Si

52 isotopes with *in-situ* techniques such as secondary ionization mass spectrometry
53 (SIMS) and laser ablation multiple collector inductively coupled plasma mass
54 spectrometry (LA-MC-ICP-MS) (e.g., [Robert and Chaussidon, 2006](#); [Shahar and](#)
55 [Young, 2007](#); [Chmeleff et al., 2008](#); [Marin-Carbonne et al., 2010](#)). SIMS measurements
56 successfully helped decipher small scale heterogeneities and processes in SiO₂-rich
57 materials and some silicates such as quartz and olivine (e.g., [Marin-Carbonne, 2014](#);
58 [Kleine et al., 2018](#); [Villeneuve et al., 2019](#)). This *in-situ* approach is required to study
59 crystals with complex histories such as zircon (ZrSiO₄) which has recently been
60 investigated by [Trail et al. \(2018\)](#) using SIMS. The major limitation of these SIMS
61 measurements is the analytical precision which is on average ~0.4‰ (2SE) and, hence,
62 prevents good resolution between a large amount of data given that high-temperature
63 processes induce limited Si isotope fractionation (e.g., [Savage et al., 2014](#)). A few
64 studies utilized LA-MC-ICP-MS to measure Si isotope signatures in rocks and minerals
65 (e.g., [Shahar and Young, 2007](#); [Chmeleff et al., 2008](#); [Ziegler et al., 2010](#); [Janney et al.,](#)
66 [2011](#); [Schuessler and Blackenburg, 2014](#); [Chen et al., 2016](#); [Frick et al., 2016](#)) and
67 consistently showed that analytical precisions can be better than 0.2‰ (2SE).
68 Therefore, LA-MC-ICP-MS could be an alternative and very likely useful technique
69 for *in-situ* studies of Si isotopes in zircon. These studies also underpinned that the type
70 of laser used (i.e., nanosecond or femtosecond) plays a very important role as SiO₂-rich
71 matrices (e.g., quartz, chert) do not always couple well with nanosecond laser beams,
72 thereby inducing poor external reproducibility (e.g., [Poitrasson and D'abzac, 2017](#)).
73 However, other types of silicate matrices, such as glass, olivine, and zircon, commonly
74 behave very well with such lasers. Given that the vast majority of LA-MC-ICP-MS
75 facilities are equipped with nanosecond lasers (excimer or solid-state), it seemed more

76 useful for the scientific community to develop Si isotope measurements using
77 nanosecond LA-MC-ICP-MS.

78 Zircon is a mineral extensively used in Earth Sciences because it can provide
79 precise geochronological information using U-Th-Pb isotope systems (e.g., [Tilton et al., 1957](#);
80 [Schoene, 2014](#)), as well as source characteristics using Hf and O isotopes
81 ([Patchett, 1983](#); [Valley, 2003](#)). In addition, it is ubiquitous in granite (*sensus largo*),
82 very resistant to weathering and erosion, and most elements diffuse very slowly within
83 its lattice ([Lee et al., 1997](#); [Cherniak and Watson, 2003, 2007](#)). Given that granite is the
84 main constituent of continents, zircon in magmatic rocks and detrital sediments has
85 long been used to study the growth of continents, which remains one of the major
86 unresolved issues in Earth Sciences (e.g., [Fedo et al., 2003](#); [Iizuka et al., 2005](#); [Guitreau
87 et al., 2012](#); [Roberts and Spencer, 2015](#)). Silicon stable isotopes have been used to
88 discriminate some granite types from others ([Savage et al., 2012](#); [André et al., 2019](#);
89 [Deng et al., 2019](#)) and their application to zircon is promising to study the growth of
90 continents, granite petrogenesis, and lithosphere-hydrosphere interactions in deep-time
91 geology ([Trail et al., 2018](#)). Theoretical work predicted that Si isotope fractionation
92 should occur between minerals and their parental melt as a function of temperature,
93 melt polymerization, mineral chemistry and Si-O bond lengths (e.g. [Méheut et al.,
94 2009](#); [Méheut and Schauble, 2014](#); [Qin et al., 2016](#)). According to [Qin et al. \(2016\)](#),
95 enrichment in ^{30}Si linked to fractionation follows the sequence quartz > albite >
96 anorthite > olivine ~ zircon > enstatite > diopside. Consequently, zircon is expected to
97 be enriched in light isotopes compared to its parental melt. This was recently confirmed
98 by measurements on natural zircons ([Trail et al., 2018](#)) as well as by experimental work
99 ([Trail et al., 2019](#)). The present contribution explores the capability of nanosecond LA-

100 MC-ICP-MS to measure Si isotopes in individual zircons for future applications in
101 Earth Sciences.

102

103 **2. Material and Methods**

104 **2.1. Standard material**

105 Reference materials in the form of glass and crystallized matrices (i.e., olivine and
106 zircon) were used for the optimization of the analytical conditions and the
107 determination of an appropriate protocol for silicon isotope measurements by LA-MC-
108 ICP-MS. Glass reference materials used in this study were SRM NIST 612, USGS
109 BHVO-2 and GSC-1G (e.g., [Jochum et al., 2005, 2011](#)). The San Carlos olivine
110 reference material (e.g., [Jarosewich et al., 1980](#)) was also investigated together with
111 zircon standards 91500 (syenite-derived; [Wiedenbeck et al., 1995](#)), MudTank
112 (carbonatite-derived; [Black and Gulson, 1978](#)), KIM (kimberlite-derived; [Valley, 2003](#);
113 [Trail et al., 2018](#)), AS3 (gabbro-derived; [Paces and Miller, 1993](#)), R33 (monzodiorite-
114 derived; [Black et al., 2004](#)), QGNG (Quartz-gabbronorite-derived; [Black et al., 2003](#)),
115 Peixe (Alkaline-rich granitoid-derived; [Chang et al., 2006](#)), Plešovice (hyperpotassic
116 granulite-derived; [Sláma et al., 2008](#)), and the artificial standards MUN from the
117 Memorial University of Newfoundland ([Fisher et al., 2011](#)).

118

119 **2.2. Measurements**

120 **2.2.1. Solution MC-ICP-MS characterization of zircon standards**

121 In order to determine the Si isotope composition of zircons and to check the validity of
122 results obtained using LA-MC-ICP-MS, we have analyzed several well-known zircon
123 reference materials using solution mode technique (S-MC-ICP-MS) modified from that
124 described in [Deng et al. \(2019\)](#). Crushed powders of 91500 and Plešovice zircons (1.5-

125 6.8 mg), as well as MUN-1 (0.6 mg), were dissolved using a NaOH fusion method
126 revised after [Georg et al. \(2006\)](#). The samples were fused in Ag crucibles with proper
127 additions of NaOH pellet (120 mg for 91500 and Plešovice zircons and only 40 mg for
128 MUN-1) at 720 °C for 15 min in a furnace. Afterwards, the glassy samples were
129 dissolved in Milli-Q H₂O by heating and ultrasonication. The samples were, then,
130 transferred into pre-cleaned tubes by Milli-Q H₂O rinsing, achieving total volumes of
131 the solutions for 91500 and Plešovice zircons to 30-40 ml and 10 ml for MUN-1 zircon.
132 This step control in dissolution volume maintains Si concentrations in the sample
133 solutions to be sufficiently high (at µg/g or sub µg/g level) for subsequent isotopic
134 measurements. For the digestions on ≥ 1 mg samples, purified 16 M HNO₃ (0.1-0.3
135 mL) were properly added to acidify the solutions until they became clear.

136 Sample aliquots containing 20 µg of Si were passed through columns hosting
137 1.8 mL BioRad AG50X-12 (200-400 meshes) cation exchange resin ([Pringle et al.,](#)
138 [2014](#)). At neutral conditions, the dissolved Si would be eluted by 5 mL Milli-Q H₂O
139 rinsing, whereas the cations would be retained on the columns by the resin. Note that
140 the resin was discarded after every single use to avoid any memory effect of any neo-
141 formed insoluble Zr particles under weak-acids. After purification, the solutions were
142 further diluted and acidified into 10 mL (2 µg/g) Si solutions in 0.2 M HNO₃. The
143 sample solutions were measured for the Si isotopic compositions on the Thermo
144 Scientific Neptune Plus multi-collector inductively coupled plasma mass spectrometer
145 (MC-ICP-MS) at the Institut de Physique du Globe de Paris (IPGP). The solutions were
146 introduced via a quartz-made spray chamber. The typical sensitivity was 10-12 V on
147 ²⁸Si⁺ for 2 µg/g of Si with an uptake rate of 100 µL/min under a medium resolution
148 mode (M/ΔM ~5000). In order to avoid isobaric interferences from ¹⁴N¹⁶O⁺ on ³⁰Si⁺,
149 the measurements of ion intensities were conducted at the lower masses of peaks 28,

150 29 and 30 (e.g., [Shahar and Young, 2007](#); [Chmeleff et al., 2008](#); [Zhang et al., 2015](#)).
151 Reference materials NBS 28 and BHVO-2 were processed following the same
152 protocols as for zircon standards, and the purified NBS 28 was used as the bracketing
153 standard. A standard-sample bracketing method was used, meaning that NBS 28
154 solutions were measured before and after each analysis of BHVO-2 and zircon
155 reference material. Each sample was analyzed 3-6 times, and each measurement
156 consisted of 25 cycles with 8.389 s of integration time per cycle. After every analysis,
157 a wash-out with 0.5 M HNO₃ and 0.2 M HNO₃ in steps was carried out. The Si blank
158 from the whole procedure was ≤ 15 ng, which is much lower than the Si masses of the
159 samples (40-2000 μ g). After Si purification, each solution was checked using Q-ICP-
160 MS and no Zr was detected whereas other elements, when detected, were all below 1
161 ppb. Note that we managed to strictly match the NO₃⁻ contents and Si concentrations
162 of the bracketing NBS 28 solutions to the corresponding sample solutions, which
163 minimizes possible matrix effects.

164

165 **2.2.2. Silicon isotope measurements by LA-MC-ICP-MS**

166 Laser ablation multiple collector inductively coupled plasma mass spectrometry
167 measurements were conducted at Laboratoire Magmas et Volcans (LMV, Clermont-
168 Ferrand, France) using a Resonetics Resolution M-50 coupled to a Thermo Scientific
169 Neptune Plus. Analytical conditions are provided in [Table 1](#). The abundance of silicon
170 isotopes was measured in high resolution mode ($M/\Delta M=7800$) and on the low-mass
171 shoulder of 28, 29, and 30 peaks to avoid isobaric interferences (e.g., [Shahar and](#)
172 [Young, 2007](#); [Chmeleff et al., 2008](#); [Janney et al., 2011](#); [Schuessler and Von](#)
173 [Blackenburg, 2014](#); [Frick et al., 2016](#)). Silicon isotope analyses were performed in
174 standard-bracketing (i.e., single measurement of an unknown bracketed by two

175 analyses of a matrix-matched standard, or batch of two unknowns bracketed by two
176 measurements of a matrix-matched standard). During the development of the
177 technique, we analyzed quartz, notably NBS 28, and silica-rich matrices (e.g., chert,
178 opale), but observed either very noisy signals or even breakage of crystals during
179 ablation. As a consequence, we could not analyze the international quartz reference
180 standard NBS 28 (NIST RM 8546) to normalize our data to. Instead, we used NIST 612
181 or the zircon standard 91500 as our normalizing reference and recalculated all data
182 relative to NBS 28. Results are reported in delta notation, $\delta^{29}\text{Si}$ and $\delta^{30}\text{Si}$, which express
183 per mil deviations from a reference, and are calculated using the following equations.

$$184 \quad \delta^x\text{Si} (\text{‰}) = \left(\frac{\left(\frac{x\text{Si}}{28\text{Si}} \right)_{\text{sample}}}{\left(\frac{x\text{Si}}{28\text{Si}} \right)_{\text{reference}}} - 1 \right) \times 1000 \quad (1)$$

185 with x being either 29 or 30. Several ways of reporting analytical uncertainties have
186 been adopted in the literature (e.g., 1 SD, 1 SE, 2 SD, 2 SE, 95% confidence). For the
187 sake of consistency, we report internal precision (i.e., within-run error or analytical
188 precision) as 2 standard-errors (2SE), also called reduced-error, which is 2 times the
189 standard-deviation divided by the square-root of the number of measurements. This is
190 the case for single zircon measurement. Note that the internal precision reported for
191 $\delta^{29}\text{Si}$ and $\delta^{30}\text{Si}$ of single measurements include a quadratic addition of the errors on the
192 bracketing standards. The external reproducibility (e.g., mean of measurements on the
193 same zircon standard) is, however, reported as 2 standard-deviations (2SD). When we
194 quote literature data and their associated uncertainties, we report them in the same way
195 as our data and, hence, recalculated them if they were reported differently in the original
196 publications. We processed Si isotope data both with and without applying background
197 correction and observed no difference in the obtained $\delta^{29}\text{Si}$ and $\delta^{30}\text{Si}$. However, data
198 that were corrected for background exhibited poorer external reproducibility likely due

199 to the limited signal-over-noise ratio (Fig. 1). As a consequence, all data presented in
200 this contribution were not corrected for background. We also applied a 2SD filter to
201 remove outliers.

202 A critical issue with high-temperature Si isotope geochemistry is the limited
203 fractionation which, in turn, results in small isotopic variability (e.g., [Savage et al. 2014](#),
204 [Deng et al., 2019](#)). This requires an appropriate analytical precision so as to be able to
205 discriminate distinct isotopic compositions. Consequently, we compared Si isotopes
206 measurements obtained by spot and line modes on synthetic glass, olivine, and zircon
207 standards. We adjusted spot size and frequency together in order to obtain highest and
208 most stable signals, and set the fluence to $\sim 3 \text{ J/cm}^2$ regardless of spot size and frequency
209 used because it corresponds to ablation conditions that are optimal for other isotope
210 systems (i.e., U-Pb and Lu-Hf; [Guitreau et al., 2019](#)).

211

212 **3. Results**

213 **3.1. S-MC-ICP-MS results**

214 Results for basalt (BHVO-2) standards are in good agreement with literature values as
215 we obtained $\delta^{29}\text{Si}$ and $\delta^{30}\text{Si}$ of -0.14 ± 0.09 and $-0.28 \pm 0.15\text{‰}$ ($n = 60$; 2SD),
216 respectively which compares well with a $\delta^{30}\text{Si} = -0.29 \pm 0.05\text{‰}$; from [Schuessler and](#)
217 [Von Blackenburg \(2014\)](#) ([Table 2](#)).

218 The two different fragments of 91500 analyzed by S-MC-ICP-MS, labeled
219 91500-MG and 91500-Corfu, exhibit very consistent $\delta^{30}\text{Si}$ values of -0.39 ± 0.10 and -
220 $0.36 \pm 0.02\text{‰}$ (2SD; [Table 2](#)). This is also true for $\delta^{29}\text{Si}$ with values of -0.19 ± 0.09 and
221 $-0.20 \pm 0.02\text{‰}$ (2SD; [Table 2](#)). The 4 different fragments of Plešovice zircon standard
222 similarly gave consistent $\delta^{30}\text{Si}$ values between -0.39 ± 0.10 and $-0.34 \pm 0.24\text{‰}$ (2SD;
223 [Table 2](#)). The artificial zircon standard MUN-1, which corresponds to MUN-1-2b from

224 MUNzirc second series (Hanchar personal communication), gave a mean $\delta^{30}\text{Si}$ value
225 of $-2.08 \pm 0.17\text{‰}$ (2SD; [Table 2](#)), which is very light compared to natural zircons. The
226 standards 91500 and Plešovice exhibit similar Si isotope values with those obtained by
227 S-MC-ICP-MS and SIMS in [Trail et al. \(2018\)](#).

228

229 **3.2. LA-MC-ICP-MS results**

230 The results are given in [Tables 3-5](#) and [S1-S5](#), and illustrated in [Figures 1-5](#). Figure 1
231 shows typical LA-MC-ICP-MS measurements of 91500 in spot and line modes and it
232 is visible that Si isotopic ratios are stable throughout a run for both modes. The spot
233 measurement (Fig. 1A) is affected by intensity decrease over the course of the analysis
234 which is due to deepening of the laser pit. On the contrary, line mode produces more
235 stable intensities that also translate into more reproducible signals and isotopic ratios.
236 Note that Si backgrounds are high which is common with laser ablation measurements.
237 [Table 3 and Figure 2](#) further show that line mode provides better internal precision and
238 external reproducibility than spot mode regardless of the type of matrix analyzed and
239 laser setting used. Such observation is consistent with those reported by [Schuessler and](#)
240 [von Blanckenburg \(2014\)](#). In order to test LA-MC-ICP-MS measurement accuracy, we
241 analyzed San Carlos olivine and 91500 zircon and used NIST 612 as a normalizing
242 reference. It can be seen in [Table 4](#) that obtained $\delta^{29}\text{Si}$ and $\delta^{30}\text{Si}$ for San Carlos and
243 91500 are inconsistent with expected values. [Schuessler and Von Blackenburg \(2014\)](#)
244 showed that differences in Si intensity between a sample and its bracketing standard
245 could result in inaccurate $\delta^{29}\text{Si}$ and $\delta^{30}\text{Si}$. The synthetic glass, NIST 612, has a much
246 higher Si concentration than olivine and zircon and, hence, we have adjusted the Si
247 intensity between San Carlos olivine and NIST 612 by changing the frequency of the
248 laser and by doing measurements in line mode. However, obtained values for San

249 Carlos olivine are still inaccurate (Table 4) which highlights the matrix-sensitive nature
250 of isotope measurements by LA-MC-ICP-MS using nanosecond lasers. Therefore, all
251 zircon analyses presented in what follows correspond to line mode (Fig. 1B) that were
252 conducted with a frequency of 6 Hz, a spot size of 33 μm , a fluence of 3 J/cm^2 , a traverse
253 rate of 1.6 $\mu\text{m}/\text{s}$, and normalized to 91500. The spot size and frequency were selected
254 to obtain the highest and most stable signal according to the MC-ICP-MS sensitivity
255 without compromising spatial resolution too much.. Data for 91500 gathered over a
256 period of more than 2 years show an external reproducibility of 0.21‰ on the self-
257 bracketed $\delta^{30}\text{Si}$ (2SD; Fig. 3), while internal precisions vary between 0.09 and 0.16‰
258 (2SE; Table S3).

259 Figure 4a illustrates that LA-MC-ICP-MS data align along a least-squares
260 regression line of 0.5132 ± 0.0034 ($R^2 = 0.98$) which falls right in between theoretical
261 predictions for mass-dependent fractionation (i.e., equilibrium = 0.5178 and kinetic =
262 0.5092; e.g. Zambardi and Poitrasson, 2011; Savage et al., 2014). Moreover, both S-
263 MC-ICP-MS and LA-MC-ICP-MS measurements have consistent fractionation
264 behavior along the terrestrial mass-dependent fractionation lines (Figure 4b). Finally,
265 Figure 5 demonstrates that our new LA-MC-ICP-MS data comply well with Si isotope
266 data obtained with other techniques on the same zircon standards (i.e., S-MC-ICP-MS
267 in this study and S-MC-ICP-MS/SIMS techniques in Trail et al., 2018).

268 Silicon isotope data for natural zircon standards overall show very little
269 variability with $\delta^{30}\text{Si}$ ranging from $-0.32 \pm 0.23\text{‰}$ for 91500 to $-0.47 \pm 0.17\text{‰}$ for
270 MudTank (2SD; Table 5). These values are consistent with Si isotope data on zircon
271 published elsewhere (Trail et al., 2018, 2019, Figure 5 and Table 5). 91500 zircon
272 analyzed in this study by LA-MC-ICP-MS and by S-MC-ICP-MS gave consistent $\delta^{30}\text{Si}$
273 of $-0.32 \pm 0.23\text{‰}$ and $-0.39 \pm 0.10\text{‰}$, respectively. AS3 zircon analyzed in this study

274 by LA-MC-ICP-MS gave a $\delta^{30}\text{Si}$ of $-0.44 \pm 0.23\text{‰}$ which is consistent within
275 uncertainty-with the value of $-0.36 \pm 0.35\text{‰}$ (2SD; [Table 5](#)) obtained by SIMS in [Trail](#)
276 [et al. \(2018\)](#). KIM zircon gave a LA-MC-ICP-MS $\delta^{30}\text{Si}$ of $-0.40 \pm 0.23\text{‰}$ identical to
277 the S-MC-ICP-MS value of $-0.41 \pm 0.01\text{‰}$ from [Trail et al. \(2018\)](#). Kuehl Lake zircon
278 gave a LA-MC-ICP-MS $\delta^{30}\text{Si}$ of $-0.38 \pm 0.12\text{‰}$ which is also consistent within
279 uncertainty with the S-MC-ICP-MS value of $-0.29 \pm 0.04\text{‰}$ published in [Trail et al.](#)
280 [\(2018\)](#). MudTank zircon displays a LA-MC-ICP-MS $\delta^{30}\text{Si}$ of $-0.47 \pm 0.17\text{‰}$ which is
281 consistent, within error, with the S-MC-ICP-MS value of $-0.34 \pm 0.03\text{‰}$ from [Trail et](#)
282 [al. \(2018\)](#). Plešovice zircon gave a LA-MC-ICP-MS $\delta^{30}\text{Si}$ of $-0.38 \pm 0.18\text{‰}$ identical
283 to S-MC-ICP-MS analyses from this study ($\delta^{30}\text{Si} = -0.39 \pm 0.06\text{‰}$). The artificial MUN
284 zircon standards exhibit consistently lighter Si isotope compositions compared to those
285 shown by natural standards. MUN zircons have slightly variable $\delta^{30}\text{Si}$ that range from
286 $-1.67 \pm 0.14\text{‰}$ for MUN-0 to $-2.05 \pm 0.30\text{‰}$ (2SD; [Table 5](#)) for MUN-4. The value of
287 $-2.00 \pm 0.22\text{‰}$ obtained for MUN-1 using LA-MC-ICP-MS ([Table 5](#)) is identical within
288 uncertainty to that obtained by S-MC-ICP-MS (i.e., $-2.08 \pm 0.17\text{‰}$; [Table 2](#)), hence,
289 confirming the enrichment of this synthetic zircon in light Si isotopes.

290

291 **4. Discussion**

292 Comparisons between Si isotope signatures of natural and synthetic zircons analyzed
293 by LA-MC-ICP-MS and S-MC-ICP-MS in this study, as well as data from the literature
294 (S-MC-ICP-MS and SIMS, [Trail et al., 2018](#)), exhibit general good consistency that
295 indicates that zircon data by LA-MC-ICP-MS are accurate and robust. Moreover,
296 although less precise than S-MC-ICP-MS analyses ($\delta^{30}\text{Si}$ within-run 2 standard error
297 of $\sim 0.02\text{-}0.05\text{‰}$), LA-MC-ICP-MS data ($\delta^{30}\text{Si}$ within-run 2 standard error of $\sim 0.10\text{-}$
298 0.15‰) are more precise than currently available SIMS data ($\delta^{30}\text{Si}$ within-run 2

299 standard error of ~0.30-0.40‰) and, hence, represent a relevant compromise between
300 precision and spatial resolution. Therefore, Si isotope measurements in zircon by LA-
301 MC-ICP-MS open new possibilities for zircon studies in various geological contexts
302 (e.g., magmatic differentiation, crustal growth).

303 This technique could be improved further in the future by reducing the high Si
304 background which is visible in [Figure 1](#) and likely influences external reproducibility
305 of Si isotope signatures. Moreover, as shown in [Zambardi and Poitrasson \(2011\)](#) silicon
306 isotopic fractionation induced by MC-ICP-MS instruments evolve non-linearly over
307 time, which requires a strict standard-bracketing procedure to be applied when
308 measuring Si isotopes by LA-MC-ICP-MS. However, if ways to stabilize the time-
309 induced drift in Si isotope ratios in MC-ICP-MS are found they would certainly help
310 improve external reproducibility of $\delta^{29}\text{Si}$ and $\delta^{30}\text{Si}$.

311 One pitfall of LA-MC-ICP-MS analysis, compared to SIMS, is the quantity of
312 material required to achieve reasonable precision. In this contribution, we have decided
313 to conduct analyses in line mode so as to obtain the best internal precision and external
314 reproducibility. In the context of zircon studies, processing by lines over spots has the
315 advantage of better coupling internal textures observed in cathodoluminescence (CL)
316 and back-scattered electron (BSE) images to the obtained isotopic information.
317 However, such lines require a rather large part of zircons to be swept across (~100 μm
318 long traverse). Possible chemical/isotopic heterogeneities may be invisible at the
319 sampling scale. One may compromise the precision for spatial resolution by doing spots
320 but would likely reduce the precision and hence the resolvability. This issue can be
321 dealt with on a case-to-case basis depending on the size and complexity of zircons
322 studied.

323

324 **5. Conclusions**

325 In this contribution, we have set up a protocol for Si isotope measurements in zircon by
326 nanosecond LA-MC-ICP-MS. Analyses performed in line mode were preferred to those
327 obtained by spot mode because of their better internal precision and external
328 reproducibility. Within-run error on zircon $\delta^{30}\text{Si}$ are on the order of $\sim 0.10\text{-}0.15\text{‰}$ (2SE)
329 and external precision of $\sim 0.15\text{-}0.30\text{‰}$ (2SD). Our LA-MC-ICP-MS data are in line
330 with those acquired with S-MC-ICP-MS and SIMS, therefore highlighting the accuracy
331 of silicon isotope measurements in zircon by LA-MC-ICP-MS. This technique,
332 therefore, offers an additional way to existing methods aiming to study zircon formation
333 in different geological contexts.

334

335 **Conflicts of interest**

336 The authors have no conflicts to declare.

337

338 **Acknowledgements**

339 Dustin Trail is thanked for providing KIM and KL zircons as well as for stimulating
340 discussions. Fernando Corfu is thanked for providing a 91500 zircon fragment. M.G.
341 acknowledges financial support from the Région Auvergne through the Auvergne
342 Fellowship program, LabEx ClerVolc (ANR-10-LABX-0006) and the French Agence
343 Nationale de la Recherche through funded ANR-JC project *Zircontinents* (ANR-17-
344 CE31-0021). This is a Laboratory of Excellence ClerVolc contribution number 418.
345 F.M. acknowledges funding from the European Research Council under the H2020
346 framework program/ERC grant agreement #637503 (Pristine). F.M. and M.C. thank the
347 financial support of the UnivEarthS Labex programme at Université de Paris (ANR-
348 10-LABX-0023 and ANR-11-IDEX-0005-02). Finally, we are grateful to Harriet

349 Brewerton for efficient editorial handling and to two anonymous reviewers who helped
350 clarify the manuscript and data presentation.

351

352 **References**

- 353 1. McDonough, W.F. Compositional model for the Earth's core. In: Holland, H.D.,
354 Turekian, K.K. (Eds.). *Treatise on Geochemistry*. Pergamon, Oxford. 2003:
355 547–568.
- 356 2. Poitrasson F. Silicon isotope geochemistry. *Reviews in Mineralogy and*
357 *Geochemistry*. 2017; 82: 289-344.
- 358 3. Ding T., Jiang S., Li Y., Gao J., Hu B. *Geochemistry of silicon isotopes*. De Gruyter.
359 2018: 279 p.
- 360 4. Sutton J.N., André L., Cardinal D., Conley D.J., de Souza G.F., Dean J., Dodd J.,
361 Ehlert C., Ellwood M.J., Frings P.J., Grasse P., Hendry K., Leng M.J.,
362 Michalopoulos P., Panizzo V.N., Swann G.E.A. A Review of the Stable Isotope
363 Bio-geochemistry of the Global Silicon Cycle and Its Associated Trace
364 Elements. *Frontiers in Earth Sciences*. 2018; 5(112): 1-24.
- 365 5. Clayton R.N., Mayeda T.K., Epstein S. Isotopic fractionation of silicon in Allende
366 inclusions. *Proceedings of the 9th Lunar and Planetary Science Conference*. 1978:
367 1267-1278.
- 368 6. Ziegler K., Chadwick O.A., White A.F., Brzezinski M.A. $\delta^{30}\text{Si}$ systematics in a
369 granitic saprolite, Puerto Rico. *Geology*. 2005; 33: 817–820.
- 370 7. André L., Cardinal D., Alleman L.Y., Moorbath S. Silicon isotopes in ~3.8 Ga West
371 Greenland rocks as clues to the Eoarchean supracrustal Si cycle. *Earth and*
372 *Planetary Science Letters*. 2006; 245: 162-173.

- 373 8. Van den Boorn S.H.J.M., van Berger M.J., Vroon P.Z., de Vries S.T., Nijman W.
374 Silicon isotope and trace element constraints on the origin of ~3.5 Ga cherts:
375 Implications for early Archaean marine environments. *Geochimica et*
376 *Cosmochimica Acta*. 2010; 74: 1077-1103.
- 377 9. Savage P.S., Georg R.B., Williams H.M., Burton K.W., Halliday A.N. Silicon
378 isotope fractionation during magmatic differentiation. *Geochimica et*
379 *Cosmochimica Acta*. 2011; 75: 6124–6139.
- 380 10. Opfergelt S., Georg R.B., Delvaux B., Cabidoche Y.-M., Burton K.W., Halliday
381 A.N. Silicon isotopes and the tracing of desilication in volcanic soil weathering
382 sequences, Guadeloupe. *Chemical Geology*. 2012; 326: 113–122.
- 383 11. Zambardi T., Poitrasson F., Corgne A., Méheut M., Quitté G., Anand M. Silicon
384 isotope variations in the inner solar system: implications for planetary
385 formation, differentiation and composition. *Geochimica et Cosmochimica Acta*.
386 2013; 121: 67–83.
- 387 12. Deng Z., Chaussidon M., Guitreau M., Puchtel I., Dauphas N., Moynier F. An
388 oceanic subduction origin for Archaean granitoids revealed by silicon isotopes.
389 *Nature Geoscience*. 2019; 12: 774-778
- 390 13. Robert F., Chaussidon M. A. Palaeotemperature curve for the Precambrian oceans
391 based on silicon isotopes in cherts. *Nature*. 2006; 443: 969-972.
- 392 14. Shahr A., Young E.D. Astrophysics of CAI formation as revealed by silicon
393 isotope LA–MC–ICPMS of an igneous CAI. *Earth and Planetary Science*
394 *Letters* 2007; 257: 497–510.
- 395 15. Chmeleff J., Horn I., Steinhöfel G., von Blanckenburg F. In situ determination of
396 precise stable Si isotope ratios by UV-femtosecond laser ablation high-resolution
397 multi-collector ICP-MS. *Chemical Geology*. 2008; 249: 155-166.

- 398 16. Marin-Carbonne J., Chaussidon M., Robert F. Microscale oxygen isotope variations
399 in 1.9 Ga Gunflint cherts: assessments of diagenesis effects and implications for
400 oceanic paleo-temperature reconstructions. *Geochimica et Cosmochimica Acta*.
401 2010; 74: 116–130.
- 402 17. Marin-Carbonne J., Robert F., Chaussidon M. The silicon and oxygen isotope
403 compositions of Precambrian cherts: A record of oceanic paleo-temperatures.
404 *Precambrian Research* 2014; 247: 223-234.
- 405 18. Kleine B.I., Stefánsson A., Halldórsson S.A., Whitehouse M.J., Jónasson K. Silicon
406 and oxygen isotopes unravel quartz formation processes in the Icelandic crust.
407 *Geochemical Perspectives Letters*. 2018; 7: 5-11.
- 408 19. Villeneuve J., Chaussidon M., Marrochi Y., Deng Z., Watson E.B. High-precision
409 in situ silicon isotopic analyses by multi-collector secondary ion mass
410 spectrometry in olivine and low-calcium pyroxene. *Rapid Communications in*
411 *Mass Spectrometry*. 2019; 33: 1589-1597.
- 412 20. Trail D., Boehnke P., Savage P. S., Liu M. C., Miller M. L., Bindeman I. Origin
413 and significance of Si and O isotope heterogeneities in Phanerozoic, Archean,
414 and Hadean zircon. *Proceedings of the National Academy of Science (USA)*.
415 2018; 115: 10287–10292.
- 416 21. Savage P.S., Armytage R.M.G., Georg R.B., Halliday A.N. High temperature
417 silicon isotope geochemistry. *Lithos*. 2014; 190-191: 500-519.
- 418 22. Ziegler K., Young E.D., Schauble E.A., Wasson J.T. Metal–silicate silicon isotope
419 fractionation in enstatite meteorites and constraints on Earth's core formation.
420 *Earth and Planetary Science Letters*. 2010; 295: 487–496.
- 421 23. Janney P.E., Richter F.M., Mendybaev R.A., Wadhwa M., Georg R.B., Watson
422 E.B., Hines R.R. Matrix effects in the analysis of Mg and Si isotope ratios in

- 423 natural and synthetic glasses by laser ablation-multicollector ICPMS: A
424 comparison of single- and double-focusing mass spectrometers. *Chemical*
425 *Geology*. 2011; 281:26-40.
- 426 24. Schuessler J.A., von Blanckenburg F. Testing the limits of micro-scale analyses of
427 Si stable isotopes by femtosecond laser ablation multicollector inductively
428 coupled plasma mass spectrometry with application to rock weathering.
429 *Spectrochimica Acta Part B*. 2014; 98: 1-18.
- 430 25. Chen X., Chafetz H.S., Andreasen R., Lapen T. Silicon isotope compositions of
431 euhedral authigenic quartz crystals: implications for abiotic fractionation at surface
432 temperatures. *Chemical Geology*. 2016; 423: 61-73.
- 433 26. Frick D.A., Schuessler J.A., von Blanckenburg F. Development of routines for
434 simultaneous in situ chemical composition and stable Si isotope ratio analysis by
435 femtosecond laser ablation inductively coupled plasma mass spectrometry.
436 *Analytica Chimica Acta*. 2016; 938: 33-43.
- 437 27. Poitrasson F., D'Abzac F.-X. Femtosecond laser ablation inductively coupled
438 plasma source mass spectrometry for elemental and isotopic analysis: are
439 ultrafast lasers worthwhile? *Journal of Analytical Atomic Spectrometry*. 2017;
440 32: 1075-1091.
- 441 28. Tilton G.R., Davis G.L., Wetherill, G.W., Aldrich L.T. Isotopic ages of zircon from
442 granites and pegmatites. *Transactions American Geophysical Union*. 1957;
443 38(3): 360-371.
- 444 29. Schoene S. U-Th-Pb geochronology. In: *Treatise on Geochemistry*, 2nd edition,
445 Elsevier, Oxford. 2014; 4.10 : 341-378.

- 446 30. Patchett P.J. Importance of the Lu–Hf isotopic system in studies of planetary
447 chronology and chemical evolution. *Geochimica et Cosmochimica Acta* 1983;
448 47: 81–91.
- 449 31. Valley J. Oxygen isotopes in zircon. *Reviews in Mineralogy and Geochemistry*.
450 2003; 53: 343-385.
- 451 32. Lee J.K.W., Williams I.S., Ellis D.J. Pb, U and Th diffusion in natural zircon.
452 *Nature*. 1997; 390:159-162.
- 453 33. Cherniak D. J., Watson, E. B. Diffusion in zircon. *Reviews in Mineralogy and*
454 *Geochemistry*, 2003; 53: 113–143.
- 455 34. Cherniak D.J., Watson, E.B. Ti diffusion in zircon. *Chemical Geology*. 2007; 242:
456 470-473.
- 457 35. Fedo C.M., Sircombe K.N., Rainbird R.H. Detrital zircon analysis of the
458 sedimentary record. *Reviews in Mineralogy and Geochemistry*, 2003; 53: 277–
459 303.
- 460 36. Iizuka T., Hirata T., Komiya T., Rino S., Katayama I., Motoki A., Maruyama, S.
461 U-Pb and Lu-Hf isotope systematics of zircons from the Mississippi river sand:
462 implications for reworking and growth of continental crust. *Geology*. 2005; 33:
463 485-488.
- 464 37. Guitreau M., Blichert-Toft J., Martin H., Mojzsis S.J., Albarède F. Hafnium isotope
465 evidence from Archean granitic rocks for deep-mantle origin of continental crust.
466 *Earth and Planetary Science Letters*. 2012; 337: 211-223.
- 467 38. Roberts N.W., Spencer C.J. The zircon archive of continent formation through time.
468 *Geological Society Special Publication*. 2015; 389: 197-225.

- 469 39. Savage P.S., Georg R.B., Williams H.M., Turner S., Halliday A.N., Chappell B.W.
470 The silicon isotope composition of granites. *Geochimica et Cosmochimica*
471 *Acta*. 2012; 92: 184–202.
- 472 40. André L., Abraham K., Hofmann A., Monin L., Kleinhanns, Foley S. Early
473 continental crust generated by reworking of basalts variably silicified by seawater.
474 *Nature Geoscience*. 2019; 12:769-773.
- 475 41. Méheut M., Lazzeri M., Balan E., Mauri F. Structural control over equilibrium
476 silicon and oxygen isotopic fractionation: A first-principles density-functional
477 theory study. *Chemical Geology*. 2009; 258: 28-37.
- 478 42. Méheut M., Schauble E.A. Silicon isotope fractionation in silicate minerals:
479 Insights from first-principles models of phyllosilicates, albite and pyrope.
480 *Geochimica et Cosmochimica Acta*. 2014, 134: 137-154.
- 481 43. Qin T., Wu F., Wu Z., Huang F. First-principles calculations of equilibrium
482 fractionation of O and Si isotopes in quartz, albite, anorthite, and zircon.
483 *Contributions to Mineralogy and Petrology*. 2016; 171: 91-104.
- 484 44. Trail D., Savage P.S., Moynier F. Experimentally determined Si isotope
485 fractionation between zircon and quartz. *Geochimica et Cosmochimica Acta*.
486 2019; 260: 257-274.
- 487 45. Jochum K.P., Willbold M., Raczek I., Stoll B., Herwig Kirstin. Chemical
488 Characterisation of the USGS Reference Glasses GSA-1G, GSC-1G, GSD-1G,
489 GSE-1G, BCR-2G, BHVO-2G and BIR-1G Using EPMA, ID-TIMS, ID-ICP-
490 MS and LA-ICP-MS. *Geostandards and Research Geoanalytical*. 2005; 29(3):
491 285-302.
- 492 46. Jochum K.P., Weis U., Stoll B., Kuzmin D., Yang Q., Raczek I., Jacob D. E.,
493 Stracke A., Birbaum K., Frick D.A., Günther D., Enzweiler J. Determination of

- 494 Reference Values for NIST SRM 610--617 Glasses Following ISO Guidelines.
495 Geostandards and Research Geoanalytical. 2011; 35(4): 397-429.
- 496 47. Jarosewich E., Nelen J.A., Norberg A. Reference samples for electron microprobe
497 analysis. Geostandards Newsletter. 1980; 4(1): 43-47.
- 498 48. Wiedenbeck M., Allé P., Corfu F., Griffin W.L., Meier M., Oberli F., von Quadt
499 A., Roddick J.C., Spiegel W. Three natural zircon standards for U–Th–Pb, Lu–
500 Hf, trace element and REE analyses. Geostandard Newsletters 1995; 19: 1–23.
- 501 49. Black L.P., Gulson, B.L. The age of the Mud Tank carbonatite, Strangways Range,
502 Northern Territory. BMR Journal of Australian Geology and Geophysics. 1978; 3:
503 227–232.
- 504 50. Paces J.B., Miller J.D. Jr. Precise U-Pb ages of Duluth Complex and related mafic
505 intrusions, Northeastern Minnesota: geochronological insights to physical,
506 petrogenetic, paleomagnetic, and tectonomagmatic processes associated with
507 the 1.1 Ga Midcontinent Rift System. Journal of Geophysical Research. 1993;
508 98: 13997-14013.
- 509 51. Black L.P., Kamo S.L., Allen C.M., Davis D.W., Aleinikoff J.N., Valley J.W.,
510 Mundil R., Campbell I.H., Korsch R.J., Williams I.S., Foudoulis C. Improved
511 $^{206}\text{Pb}/^{238}\text{U}$ microprobe geochronology by the monitoring of a trace-element-related
512 matrix effect; SHRIMP, ID-TIMS, ELA-ICP-MS and oxygen isotope
513 documentation for a series of zircon standards. Chemical Geology. 2004; 205: 115-
514 140.
- 515 52. Black L.P., Kamo S.L., Williams I.S., Mundil R., Davis D.W., Korsch R.J.,
516 Foudoulis C. The application of SHRIMP to Phanerozoic geochronology; a critical
517 appraisal of four zircon standards. Chemical Geology. 2003; 200: 171-188.

- 518 53. Chang Z., Vervoort J.D., McClelland W.C., Knaack C. U-Pb dating of zircon by
519 LA-ICP-MS. *G-Cubed*. 2006; 7(5): 1-14.
- 520 54. Sláma, J., J. Košler, D.J. Condon, J.L. Crowley, A. Gerdes, J.M. Hanchar, M.S.A.
521 Horstwood, G.A. Morris, L. Nasdala, N. Norberg, U. Schaltegger, B. Schoene,
522 M.N. Tubrett, and M.J. Whitehouse. Plesovice zircon -- A new natural reference
523 material for U-Pb and Hf isotopic microanalysis. *Chemical Geology*. 2008; 249:
524 1-35.
- 525 55. Fisher C.M., Hanchar J.M., Samson S.D., Dhuime B., Blichert-Toft J., Vervoort
526 J.D., Lam R. Synthetic zircon doped with hafnium and rare earth elements: A
527 reference material for in situ hafnium isotope analysis. *Chemical Geology*. 2011;
528 286: 32-47.
- 529 56. Georg, R. B., Reynolds, B. C., Frank, M. & Halliday, A. N. New sample preparation
530 techniques for the determination of Si isotopic compositions using MC-ICPMS.
531 *Chemical Geology*. 2006; 235: 95–104.
- 532 57. Pringle E. A., Moynier F., Savage P. S., Badro J., Barrat J. A. Silicon isotopes in
533 angrites and volatile loss in planetesimals. *Proceedings of the National*
534 *Academy of Science (USA)*. 2014; 111: 17029–17032.
- 535 58. Zhang A.-Y., Zhang J., Zhang R.-F., Xue Y. Determination of stable silicon
536 isotopes using multi-collector inductively coupled plasma mass spectrometry.
537 *Chinese journal of analytical chemistry*. 2015; 43(9): 1353-1359.
- 538 59. Guitreau M., Boyet M., Paquette J.-L., Gannoun A., Konc Z., Benbakkar M.,
539 Suchorski K., Hénot J.-M. Hadean protocrust reworking at the origin of the Napier
540 Complex (Antarctica). *Geochemical Perspectives Letters*. 2019; 12, 7-11.

541 60. Zambardi T., Poitrasson F. Precise determination of silicon isotopes in silicate rock
542 reference materials by MC-ICP-MS. *Geostandards and Geoanalytical Research*.
543 2011; 35: 89–99.

544

545 **Figure and Table captions**

546 Table 1. LA-MC-ICP-MS operating conditions

547

548 Table 2. Silicon isotope results for zircons analyzed by S-MC-ICP-MS

549

550 Table 3. External reproducibility of self-normalized standards

551

552 Table 4. Summary of Si isotope measurements by LA-MC-ICP-MS of San Carlos and
553 91500 normalized to NIST 612

554

555 Table 5. Silicon isotope results for zircons analyzed by LA-MC-ICP-MS

556

557 Figure 1. Signal and isotope ratio evolutions throughout a typical analysis of the zircon
558 standard 91500 in spot (A) and line (B) modes using the same analytical conditions
559 (i.e., spot size of 33 μm , frequency of 6 Hz, fluence of 3 J/cm^2 and sweeping rate of
560 1.6 $\mu\text{m}/\text{s}$ for the line mode, and). In the insets, $\delta^{29}\text{Si}$ and $\delta^{30}\text{Si}$ values were calculated
561 by normalization to the average $^{29}\text{Si}/^{28}\text{Si}$ and $^{30}\text{Si}/^{28}\text{Si}$ of the corresponding analysis.
562 Note that during ablation both the isotope ratios are stable, despite high intensities of
563 Si in the background (laser off)..

564

565 Figure 2. External reproducibility of Si isotopes in different matrices. Delta values are
566 self-normalized for each standard. Note the general better external reproducibility of
567 line analyses compared to spots regardless of the matrix analyzed

568

569 Figure 3. Long-term (>2 years) reproducibility of Si isotope signatures in 91500 (self-
570 bracketed).

571

572 Figure 4. Silicon isotope results for zircon analysed by LA-MC-ICP-MS and S-MC-
573 ICP-MS. Figure A shows the relationship between $\delta^{29}\text{Si}$ and $\delta^{30}\text{Si}$ for all single LA-
574 MC-ICP-MS measurements whereas B exhibits the relationship between $\delta^{29}\text{Si}$ and
575 $\delta^{30}\text{Si}$ for averages of all zircon standards analyzed by LA-MC-ICP-MS and S-MC-ICP-
576 MS. Note that MUN artificial zircon standards have very light Si isotope signatures
577 compared to natural zircons and that data align along the terrestrial mass-dependent
578 fractionation lines, labeled EMFL and KMFL for equilibrium and kinetic fractionation,
579 respectively.

580

581 Figure 5. Comparison between LA-MC-ICP-MS and S-MC-ICP-MS/SIMS data for
582 zircon standards (MUN-1, 91500, AS3, KIM, Kuehl Lake, MudTank, and Plešovice)
583 from this study and [Trail et al. \(2018\)](#). All data align along a line with a slope of 1,
584 therefore, indicating very good agreement between techniques.

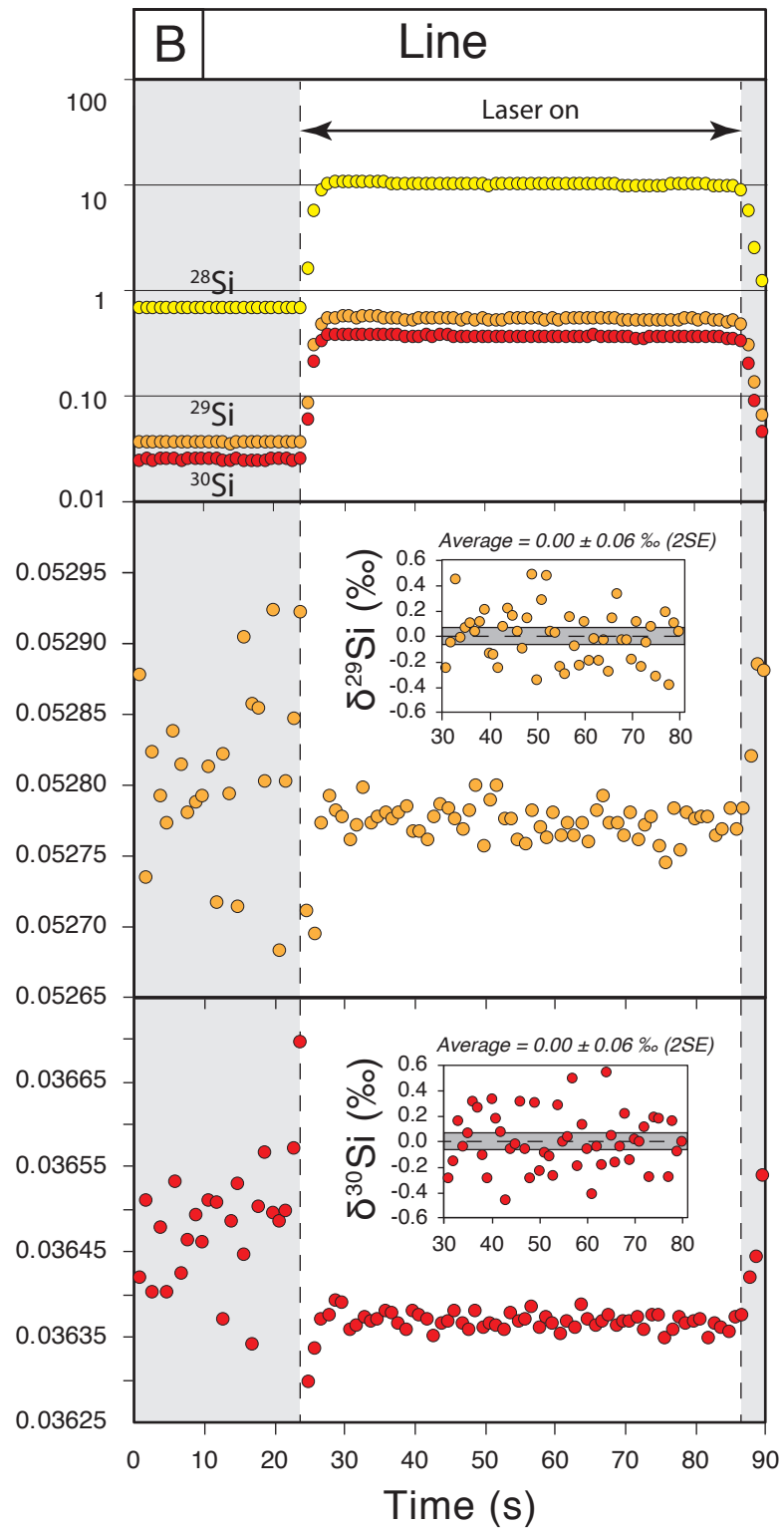
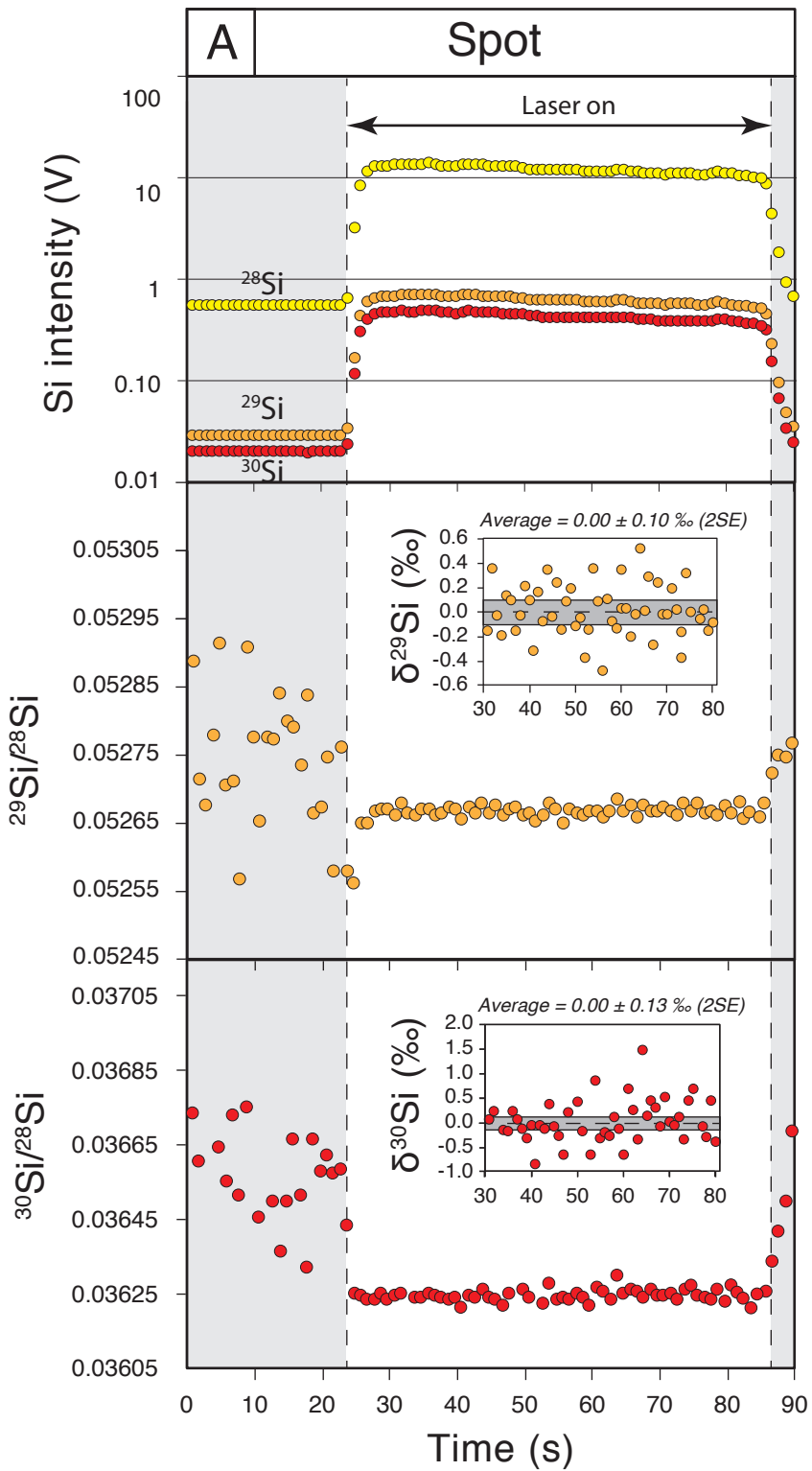
585

586 **Supplementary Table captions**

587 Table S1. All LA-MC-ICP-MS results for standards

588 Table S2. Results for Si isotope measurements by LA-MC-ICP-MS of San Carlos
589 olivine and 91500 zircon normalized to NIST 612

590 Table S3. All results for 91500 (self-bracketed) analyzed by LA-MC-ICP-MS in line
591 mode
592 Table S4. All Si isotope data for zircon analyzed by LA-MC-ICP-MS in line mode
593 Table S5. All raw LA-MC-ICP-MS data



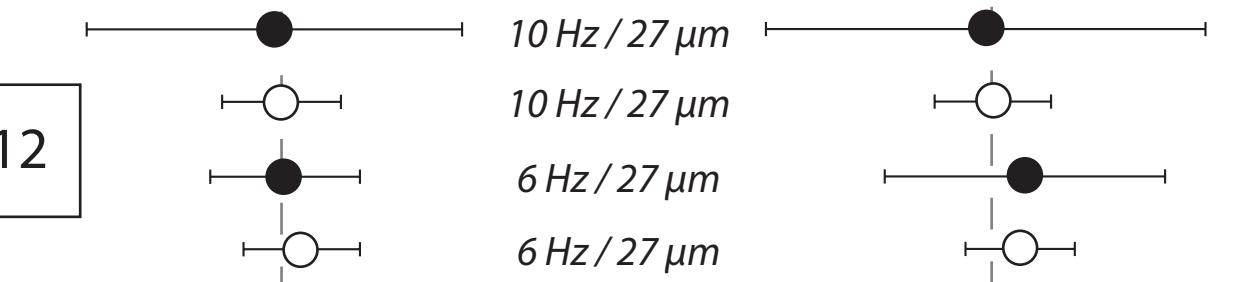
$\delta^{29}\text{Si}$ (‰) self-normalized

$\delta^{30}\text{Si}$ (‰) self-normalized

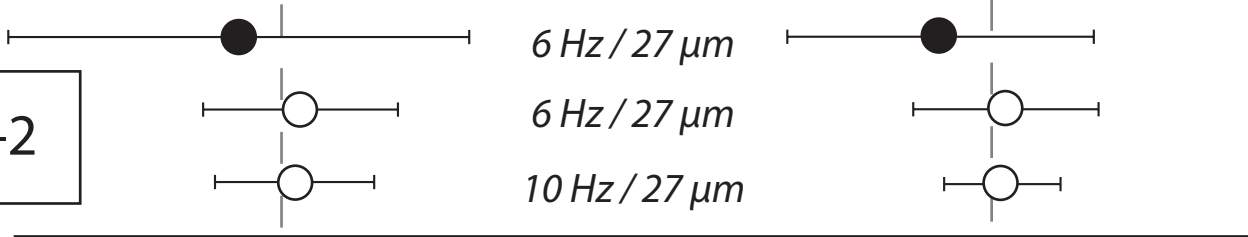
-0.6 -0.4 -0.2 0.0 0.2 0.4

-0.8 -0.4 0.0 0.4 0.8

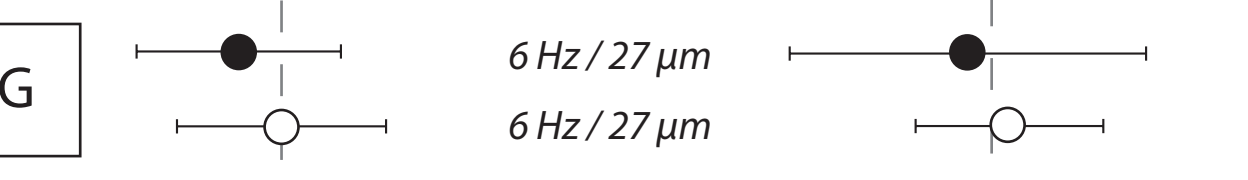
NIST 612



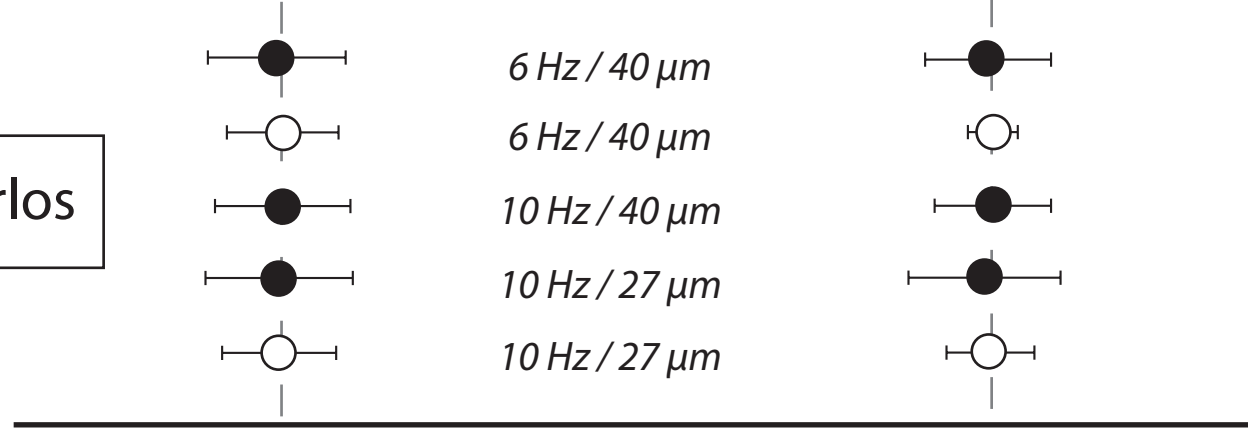
BHVO-2



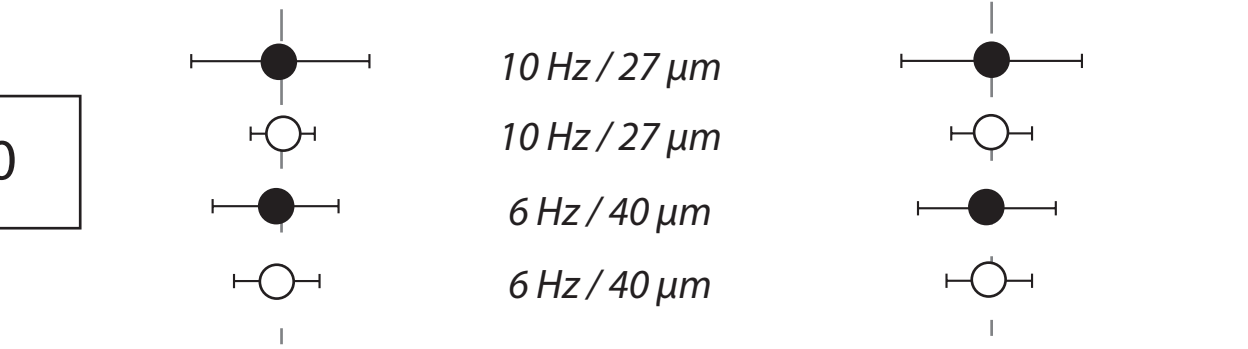
GSC-1G



San Carlos



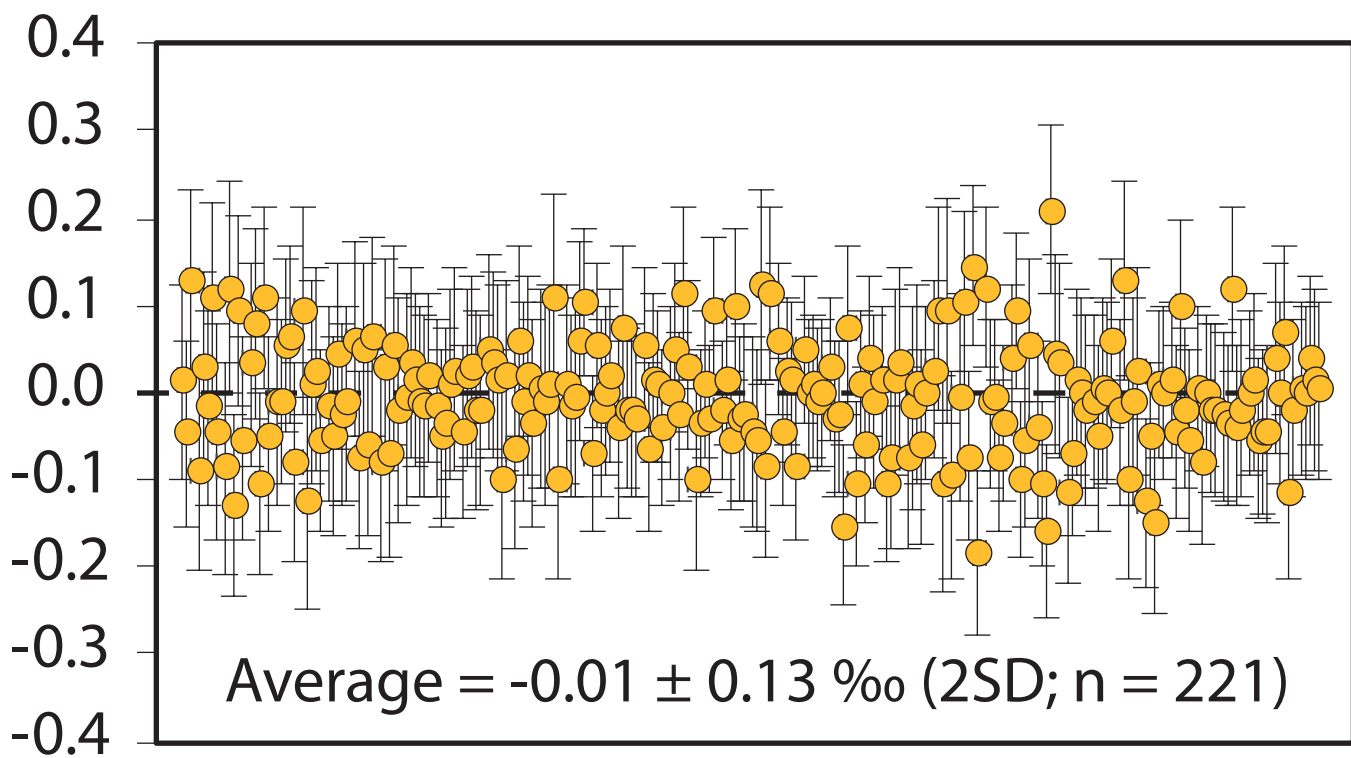
91500



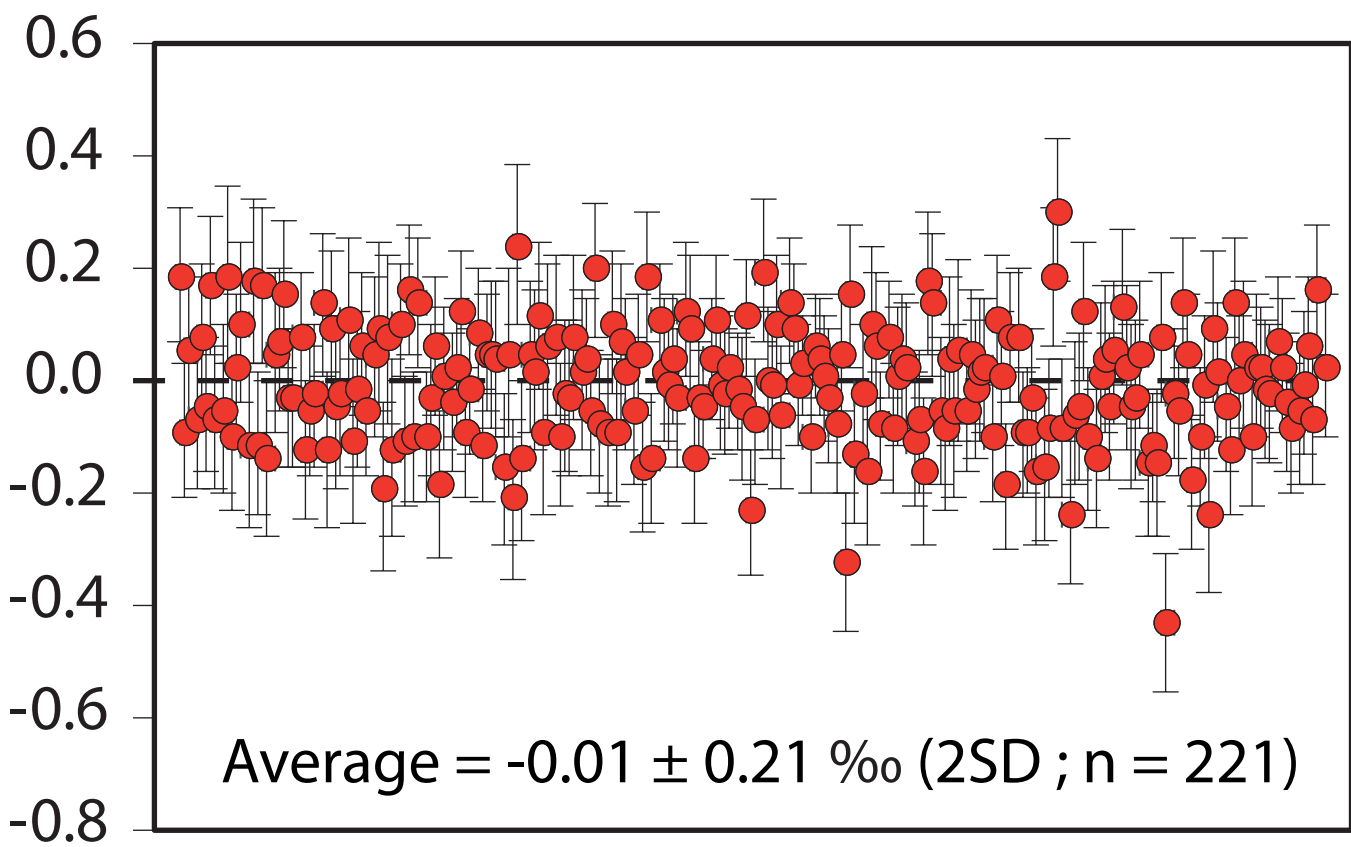
○ Line ● Spot

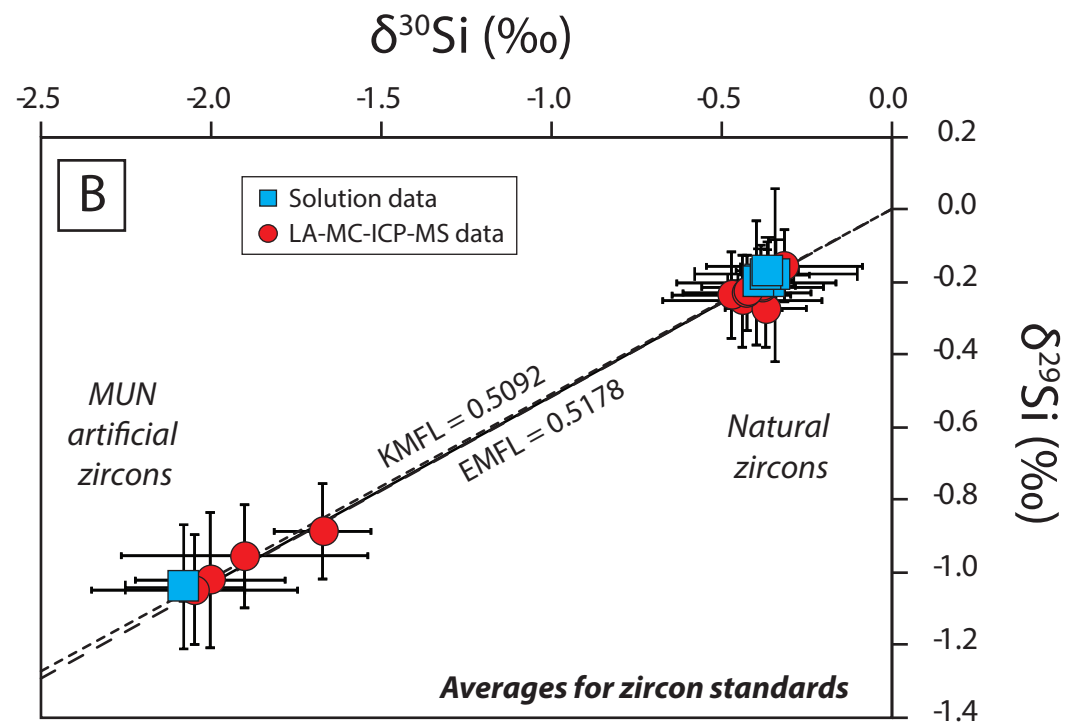
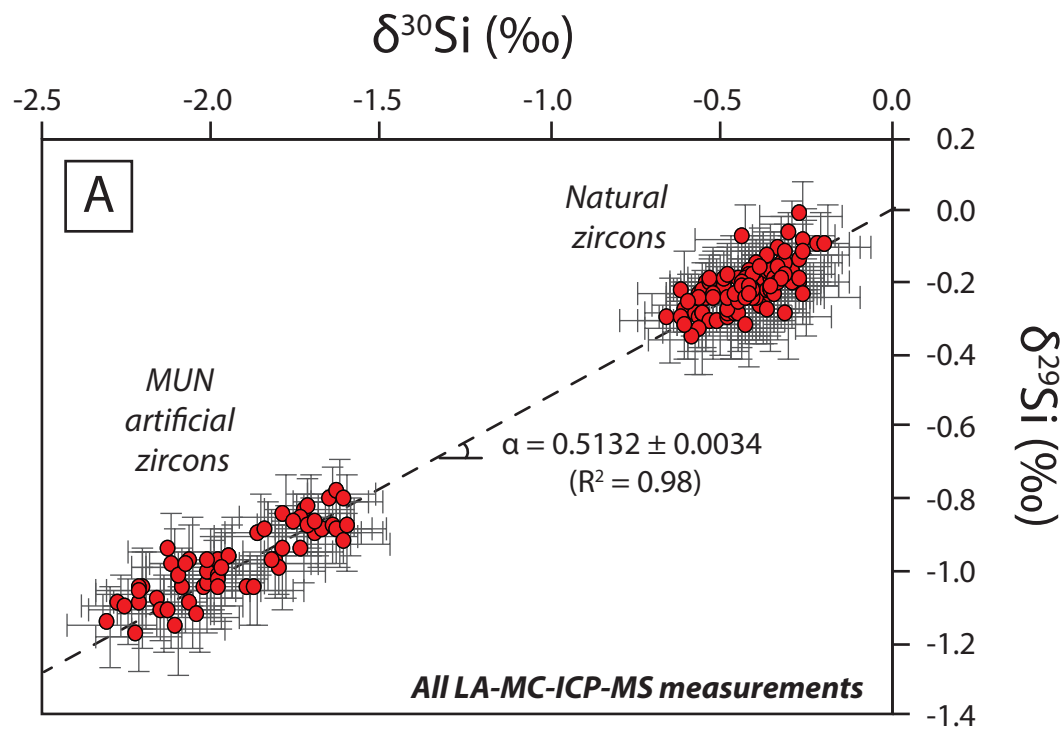
91500 zircon standard

$\delta^{29}\text{Si}$ (‰) self-normalized



$\delta^{30}\text{Si}$ (‰) self-normalized





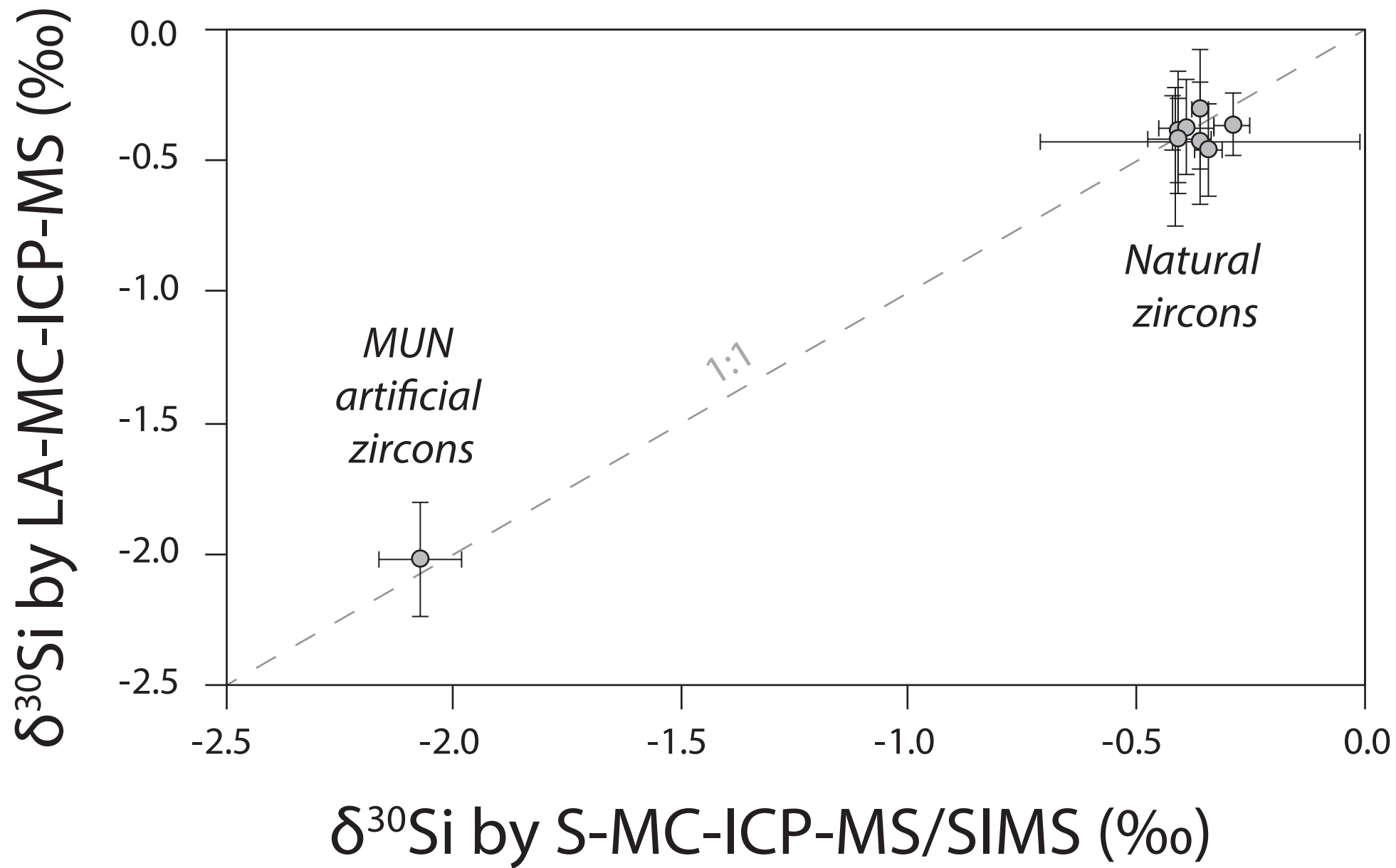


Table 1. LA-MC-ICP-MS operating conditions

Analysis	<i>Si isotopes</i>		
Laboratory	Magmas et Volcans		
Cup configuration	L3	C	H3
Mass measured	28	29	30
MC-ICP-MS model	Thermo Neptune <i>Plus</i>		
Interface type	Jet (high sensitivity)		
Cones	X-Cones		
Resistors	10 ¹¹ Ohms		
Resolution	High (M/ΔM~7800)		
Forward Power	1200 W		
Auxiliary gas (Ar)	0.7-0.8 L/min		
Ar sample	0.9-1.1 L/min		
SQUID	On		
Data acquisition	Time resolved analysis		
Scanning mode	Static multi-collection		
Integration time per isotope	1s		
Background counting time	20-30 s		
Sample measurement time	40-60s		
Measurement type	Standard bracketing		
External standard	NIST 612, 91500		
Laser model	Resonetics Resolution M-50E		
Wavelength	193 nm		
Pulse duration	5 ns		
Energy	2-5 mJ		
Fluence	~3 J/cm ²		
Frequency	6-10 Hz		
Spot size	27-40 μm		
Carrier gas	He		
Carrier gas flow	0.65-0.75 L/min		
Traverse rate	1.6 μm/s		

Table 2. Si isotope results for zircons analyzed by S-MC-ICP-MS

Sample	$\delta^{29}\text{Si}^*$ (‰)	2SD	$\delta^{30}\text{Si}^*$ (‰)	2SD	n
NBS 28 (NIST 8546)	0.00	0.08	0.00	0.13	236
BHVO-2	-0.14	0.09	-0.28	0.15	60
91500-MG	-0.19	0.09	-0.39	0.10	4
91500-Corfu	-0.20	0.02	-0.36	0.02	4
Plešovice-MG	-0.20	0.06	-0.39	0.06	4
Plešovice-IPGP	-0.18	0.10	-0.34	0.24	4
Plešovice-IPGP	-0.18	0.03	-0.37	0.07	4
Plešovice-IPGP	-0.17	0.09	-0.37	0.08	4
MUN-1	-1.04	0.04	-2.08	0.17	4

* normalized to NBS 28

Table 3. External reproducibility of self-normalized standards

Name	$\delta^{29}\text{Si}$ 2SD	$\delta^{30}\text{Si}$ 2SD	Analysis	Repetition rate	Spot size	Fluence	n	
NIST 612	-0.01	0.35	-0.02	0.83 Spot	10 Hz	27 μm	$\sim 3 \text{ J.cm}^{-2}$	4
NIST 612	0.00	0.11	0.01	0.22 Line	6 Hz	27 μm	$\sim 3 \text{ J.cm}^{-2}$	9
NIST 612	0.01	0.14	0.13	0.52 Spot	6 Hz	27 μm	$\sim 3 \text{ J.cm}^{-2}$	9
NIST 612	0.04	0.11	0.11	0.20 Line	6 Hz	27 μm	$\sim 3 \text{ J.cm}^{-2}$	9
BHVO-2	-0.08	0.43	-0.19	0.57 Spot	6 Hz	27 μm	$\sim 3 \text{ J.cm}^{-2}$	4
BHVO-2	0.03	0.18	0.06	0.35 Line	6 Hz	27 μm	$\sim 3 \text{ J.cm}^{-2}$	6
BHVO-2	0.02	0.15	0.04	0.22 Line	10 Hz	27 μm	$\sim 3 \text{ J.cm}^{-2}$	8
GSC-1G	-0.08	0.19	-0.09	0.67 Spot	6 Hz	27 μm	$\sim 3 \text{ J.cm}^{-2}$	4
GSC-1G	0.00	0.20	0.07	0.35 Line	6 Hz	27 μm	$\sim 3 \text{ J.cm}^{-2}$	6
San Carlos	-0.01	0.13	-0.01	0.24 Spot	6 Hz	40 μm	$\sim 3 \text{ J.cm}^{-2}$	9
San Carlos	0.00	0.10	0.00	0.09 Line	6 Hz	40 μm	$\sim 3 \text{ J.cm}^{-2}$	9
San Carlos	-0.01	0.14	-0.02	0.29 Spot	10 Hz	27 μm	$\sim 3 \text{ J.cm}^{-2}$	9
San Carlos	-0.01	0.11	-0.01	0.17 Line	10 Hz	27 μm	$\sim 3 \text{ J.cm}^{-2}$	15
San Carlos	0.00	0.13	0.01	0.22 Spot	10 Hz	40 μm	$\sim 3 \text{ J.cm}^{-2}$	9
91500	0.00	0.17	0.00	0.34 Spot	10 Hz	27 μm	$\sim 3 \text{ J.cm}^{-2}$	9
91500	0.00	0.06	0.00	0.15 Line	10 Hz	27 μm	$\sim 3 \text{ J.cm}^{-2}$	9
91500	-0.01	0.12	-0.02	0.26 Spot	6 Hz	40 μm	$\sim 3 \text{ J.cm}^{-2}$	9
91500	-0.01	0.08	-0.01	0.16 Line	6 Hz	40 μm	$\sim 3 \text{ J.cm}^{-2}$	9
91500	-0.01	0.13	-0.01	0.21 Line	6 Hz	33 μm	$\sim 3 \text{ J.cm}^{-2}$	221

Table 4 - Summary of Si isotope measurements by LA-MC-ICP-MS of San Carlos and 91500 normalized to NIST 612

Average	Sample				Laser setup	Mode	Si _S /Si _{NIST} **	Literature				
	δ ²⁹ Si(‰)*	2 SD	δ ³⁰ Si(‰)*	2 SD				δ ²⁹ Si(‰)***	2 SD	δ ³⁰ Si(‰)***	2 SD	Reference
San Carlos	-0.74	0.20	-1.44	0.51	6 Hz 40 μm	Spot	0.5	-0.20	0.10	-0.34	0.15	Schuessler and Von Blackenburg (2014)
San Carlos	-0.85	0.11	-1.67	0.43	10 Hz 27 μm	Spot	0.6	-0.20	0.10	-0.34	0.15	Schuessler and Von Blackenburg (2014)
San Carlos	-0.60	0.08	-1.19	0.22	10 Hz 27 μm	Raster	0.9	-0.20	0.10	-0.34	0.15	Schuessler and Von Blackenburg (2014)
91500	0.19	0.17	0.37	0.21	6 Hz 40 μm	Spot	0.6	-0.20	0.02	-0.36	0.02	<i>This study</i>
91500	0.00	0.31	-0.12	0.48	10 Hz 27 μm	Spot	0.7	-0.20	0.02	-0.36	0.02	<i>This study</i>

* Delta values are relative to NBS 28 but normalized to NIST 612 that was analyzed in the same conditions except for the rasters for which NIST 612 was analyzed using 6 Hz and 27 μm.

** S refers to sample (San Carlos or 91500) and NIST to NIST 612.

*** Delta values are relative to NBS 28

Table 5. Si isotope results for zircons analyzed by LA-MC-ICP-MS

Technique	Sample	$\delta^{29}\text{Si}^*$ (‰)				$\delta^{30}\text{Si}^*$ (‰)				<i>Data from other techniques</i>		
		2SD	2SD	2SD	n	Technique	$\delta^{30}\text{Si}^*$ (‰)	2SD	Reference			
LA-MC-ICP-MS	91500-MG	-0.15	0.10	-0.32	0.23	5	S-MC-ICP-MS	-0.39	0.10	<i>This study</i>		
LA-MC-ICP-MS	AS3	-0.25	0.13	-0.44	0.23	28	SIMS	-0.36	0.35	Trail et al. (2018)		
LA-MC-ICP-MS	KIM	-0.20	0.17	-0.40	0.23	16	S-MC-ICP-MS	-0.41	0.01	Trail et al. (2018)		
LA-MC-ICP-MS	Kuehl Lake	-0.25	0.11	-0.38	0.12	3	S-MC-ICP-MS	-0.29	0.04	Trail et al. (2018)		
LA-MC-ICP-MS	MudTank	-0.23	0.12	-0.47	0.17	13	S-MC-ICP-MS	-0.34	0.03	Trail et al. (2018)		
LA-MC-ICP-MS	MUN-0	-0.88	0.13	-1.67	0.14	14	-	-	-	-		
LA-MC-ICP-MS	MUN-1	-1.02	0.19	-2.00	0.22	8	S-MC-ICP-MS	-2.08	0.17	<i>This study</i>		
LA-MC-ICP-MS	MUN-3	-0.95	0.14	-1.90	0.36	10	-	-	-	-		
LA-MC-ICP-MS	MUN-4	-1.05	0.15	-2.05	0.30	25	-	-	-	-		
LA-MC-ICP-MS	Peixe	-0.23	0.10	-0.43	0.19	11	-	-	-	-		
LA-MC-ICP-MS	Plešovice-MG	-0.21	0.07	-0.38	0.18	11	S-MC-ICP-MS	-0.39	0.06	<i>This study</i>		
LA-MC-ICP-MS	QGNG	-0.21	0.05	-0.38	0.10	7	-	-	-	-		
LA-MC-ICP-MS	R33	-0.22	0.04	-0.42	0.08	8	-	-	-	-		

* relative to NBS 28